LAWRENCE
LIVERMORE
NATIONAL
LABORATORY

LLNL-JRNL-496612

Origin and role of magnetic stochasticity in plasma microturbulence

D. R. Hatch, M. J. Pueschel, W. M. Nevins, F. Jenko, P. W. Terry, H. Doerk

August 30, 2011

Physical Review Letters

Disclaimer

Origin and role of magnetic stochasticity in plasma microturbulence

D.R. Hatch,[1,2] M. J. Pueschel,[2] W. M. Nevins,[3] F. Jenko,[2] P. W. Terry,[1] and H. Doerk[2]

[1] *University of Wisconsin-Madison, Madison, Wisconsin 53706, USA*
[2] *Max-Planck-Institut für Plasmaphysik, EURATOM Association, 85748 Garching, Germany*
[3] *Lawrence Livermore National Laboratory, Livermore, California 94550, USA*

Recent studies have shown that magnetic stochasticity is near-ubiquitous in electromagnetic gyrokinetic simulations. This occurs even when the turbulence is driven by modes that are characterized by ballooning (rather than tearing) parity. We show that the magnetic stochasticity and associated transport are produced by nonlinearly-driven, subdominant microtearing modes. The nonlinear excitation mechanism and a simple model describing the β dependence of the electromagnetic transport are also described.

PACS numbers: 52.35.Hr,52.35.Ra,52.65.Tt

The inclusion of electromagnetic effects in gyrokinetic simulations allows the magnetic field to evolve self-consistently with the other fluctuations and produces additional transport channels wherein heat may be transported radially via electrons streaming along perturbed field lines. Over the last several years significant progress has been made in understanding electromagnetic effects in plasma microturbulence [1]-[5]. Recent studies [3, 4] have examined scans in β centered on the Cyclone Base Case (CBC) [6] parameters, showing that the electron electromagnetic transport increases roughly with β^2 until it achieves a value that is on the same order as the electrostatic contributions. Recently, magnetic fluctuations in a CBC β scan have been shown to produce stochastic magnetic fields even at very low values of β [7–9]. This fully developed stochasticity has been somewhat puzzling in light of the fact that the driving instabilities in these parameter regimes are characterized by ballooning (and not tearing) parity, i.e., the magnetic vector potential, $A_{||}$, is an odd function of the extended ballooning angle and thus can merely bend but not break field lines. In this letter we describe the underlying mechanism for this stochasticity and the associated electron heat transport. Using simulation data produced by the GENE code [1], we show here that the stochasticity is caused not by the unstable modes which drive the turbulence, but rather subdominant microtearing modes. These modes are excited primarily through nonlinear interaction with zonal wavenumbers ($k_y = 0$). This defines a novel scenario in which zonal modes play a dual role, as not only the well-known saturation mechanism for the instability, but also the catalyst of an additional transport channel.

This study builds upon a body of work which has explored the role of damped eigenmodes in plasma microturbulence [10–12]. It is also related to recent studies which model, via gyrokinetic simulations, turbulence driven by unstable microtearing modes [13, 14]. Here we show that such modes need not be dominant or even unstable to produce significant levels of transport.

Much of the data used in this analysis is taken from the GENE dataset described in Ref. [4]. The CBC parameters are used, with the addition of finite electron plasma $\beta = 8\pi n_e T_e / B_0^2$ ranging from the electrostatic limit to $\beta = 0.012$. The reader is referred to Ref. [4] for a detailed description of the physical and numerical parameters.

First we demonstrate the presence of tearing structures in the turbulent magnetic fluctuations and show that these structures are responsible for the observed magnetic stochasticity and transport. In order to do this we construct proper orthogonal decompositions (POD) [15] of the fluctuating $A_{||}$. This application of POD is similar to those reported in Refs. [11, 12, 16]. It decomposes the magnetic fluctuations as a superposition of fixed mode structures whose amplitudes fluctuate in time: $A_{||}(z,t) = \sum_n A_{||}^{(n)}(z) h^{(n)}(t)$. Both the mode structures, $A_{||}^{(n)}(z)$, and the time traces, $h^{(n)}(t)$, are orthogonal, and are arranged in order of decreasing amplitude.

In order to study the contribution of different processes to the dynamics of the magnetic fluctuations, we seek to decompose $A_{||}$ into components corresponding to the dominant ballooning parity modes (ITG) and the subdominant tearing modes. We do this by constructing a POD of every linearly independent set of wavenumbers in the full $A_{||_{k_x,k_y}}(z,t)$ dataset. A linearly independent set of wavenumbers consists of a single k_y wavenumber, and all k_x wavenumbers that define its extended ballooning structure. These k_x modes are connected by the flux tube parallel boundary condition [17] and are identical to the k_x modes that are resolved in a corresponding linear simulation. It is observed that the $n = 1$ POD mode structure matches very closely the mode structure of the unstable ITG mode at wavenumbers with strong linear drive. This is an indication of the effectiveness of this analysis in separating the role of the most unstable ITG modes from that of the subdominant tearing modes. The first two $A_{||}$ POD modes almost invariably define a clear ballooning component (odd in z) and a clear tearing component (even in z). An example is shown in Fig. 1, where the $n = 1$ and $n = 2$ modes are plotted for $k_y \rho_s = 0.2, k_x \rho_s = 0$, and $\beta = 0.003$. As will be shown,

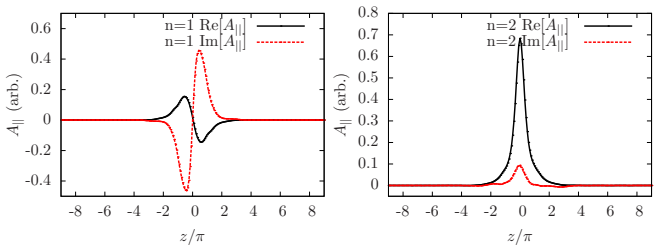

FIG. 1: Typical $A_{||}$ POD modes structures. The $n = 1$ mode (left) has ballooning parity and the $n = 2$ mode (right) has tearing parity.

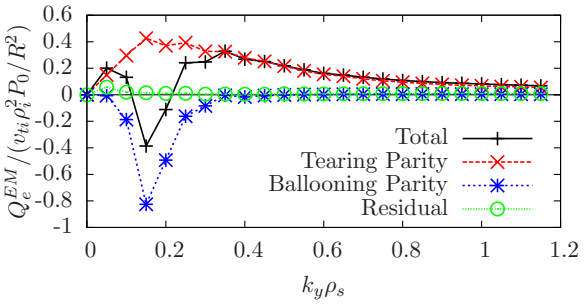

FIG. 2: The total electromagnetic electron heat flux spectrum (plus signs), summed over k_x for $\beta = 0.003$, decomposed into contributions from tearing modes (crosses), ballooning modes (asterisks) and all remaining fluctuations (circles).

nearly all of the important effects of the magnetic fluctuations can be captured with only these two modes (i.e., the first two POD modes for each wavenumber).

When the central k_x value is non-zero, the modes may peak at the corresponding non-zero ballooning angle and also exhibit some mixing of the parity in a fashion similar to that observed in the linear modes. Even in these cases, there typically remains one mode which is predominantly tearing and one which is predominantly ballooning. In order to automatically distinguish the ballooning components from the tearing components, a parity factor is defined, $P = |\int dz A_{||}|/\int dz|A_{||}|$. The parity factor is zero for pure ballooning parity and may approach a value of one for tearing parity modes. This can be used to decompose the entire $A_{||}$ dataset as follows,

$$A_{||_{k_x,k_y}}(z,t) = A_{||}^{(ball)} + A_{||}^{(tear)} + A_{||}^{(res)}, \qquad (1)$$

where the ballooning component (*ball*) is defined as whichever of the first two POD modes has the smaller parity factor, the tearing component (*tear*) is whichever of the first two POD modes has the larger parity factor, and the rest of the POD modes are grouped into the residual category (*res*).

This analysis procedure can be summarized as follows: 1. Select from the $A_{||}$ fluctuation data a single k_x and k_y, along with all k_x modes connected by the parallel boundary condition. 2. Construct a POD of this data set. 3. Select from the first two POD modes the one with the largest parity factor and group it in the tearing component of the decomposition. 4. Select from the first two POD modes the one with the smaller parity factor and group it in the ballooning component of the decomposition. 5. Repeat steps 1-4 for all sets of wavenumbers in the dataset. The result is a decomposition [as defined in Eq. (1)] of the entire $A_{||_{k_x,k_y}}(z,t)$ which defines a dominant ballooning component, a dominant tearing component and all other residual fluctuations.

With this tearing-ballooning decomposition in hand, we can study the contribution of each component to the magnetic field fluctuations and transport. In order to do this, a routine is used to follow the trajectory of magnetic field lines and track their deviation from the equilibrium field. This can be quantified with a magnetic diffusivity $D_{fl} = \lim_{l\to\infty} \langle [r_i(l) - r_i(0)]^2 \rangle / l$ [8]. Across the β scan, the tearing component of $A_{||}$ produces a magnetic diffusivity that is comparable to that of the total $A_{||}$, while the ballooning and residual components produce comparatively negligible diffusivities.

In Refs. [8, 9], the magnetic diffusivity is shown to have quite a direct relation to the electron electromagnetic heat transport. Using the tearing-ballooning decomposition we can directly calculate different contributions to Q_e^{EM}. The Q_e^{EM} k_y spectra are quite distinctive (see, e.g., Fig. 6b in Ref. [3]); they exhibit a dip in the flux at the same scales where the dominant transport channel (Q_i^{ES}) peaks ($0.1 \lesssim |k_y\rho_s| \lesssim 0.3$). This dip dominates at low β and becomes less prominent as β increases. The present analysis shows that this feature is the result of the superposition of the transport associated with the ITG modes and the stochastic transport associated with the subdominant tearing modes, as will be described below.

Using the decomposition defined in Eq. (1), one can define a ballooning component of the flux, $Q_e^{EM}[A_{||}^{ball}, q_{||}]$, a tearing component, $Q_e^{EM}[A_{||}^{tear}, q_{||}]$, and the residual, $Q_e^{EM}[A_{||}^{res}, q_{||}]$. Note that in these expressions $A_{||}$ has been decomposed into the different classes of magnetic fluctuations, but the parallel heat flux moment, $q_{||}$, is not decomposed. The k_y flux spectra (at $\beta = 0.003$) for the different components are shown in Fig. 2. The ballooning component of the flux defines a heat pinch that peaks in the low k_y region where the ITG modes dominate. In contrast, the tearing component of the transport is outward, also peaking at low k_y, but additionally extending with significant amplitude to the higher wavenumbers in the spectrum. The total transport spectrum is a superposition of these two contributions. For the $\beta = 0.003$ value shown here, the two components are similar in magnitude. The ballooning transport follows roughly the quasilinear expectation, scaling like β [4]. The tearing component, on the other hand, follows a β^2

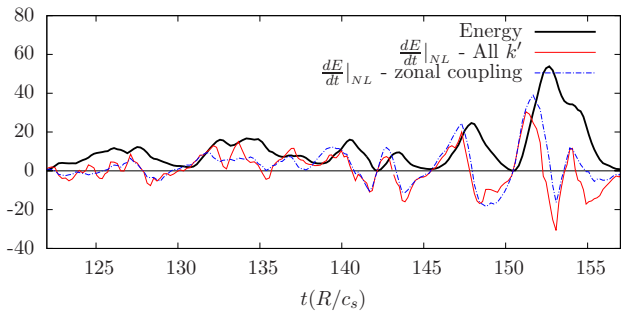

FIG. 3: The free energy in the POD tearing mode (black) at $k_x\rho_s = 0, k_y\rho_s = 0.2$, and $\beta = 0.003$ along with the total nonlinear drive (red) and the nonlinear drive defined by coupling with zonal wavenumbers (blue), plotted over a time segment of the nonlinear saturated state. The energetics of the tearing mode is dominated by the nonlinear drive which consists largely of the zonal coupling.

dependence and thus dominates as β increases.

Having demonstrated the role of tearing structures in the magnetic stochasticity and transport, we turn now to identifying an excitation mechanism. To this end, we first construct a POD of the gyrocenter distribution function from a GENE simulation and examine the energetics of the tearing fluctuations. We examine in detail the wavenumber $k_y\rho_s = 0.2, k_x\rho_s = 0$ for the $\beta = 0.003$ case. The $n = 4$ mode in the POD exhibits clear tearing parity and also defines the dominant outward contribution to the electromagnetic heat flux. In order to examine the excitation mechanism of this mode we construct nonlinear energy transfer functions [18]. The free energy is defined as $E_k = \sum_j \int dz dv_{||} d\mu \left(g_{k_j} + q_j F_0/T_{0j}\chi_{k_j}\right)^* g_{k_j}$, where j denotes the particle species, g_j is the gyrocenter distribution function, q_j is particle charge, F_0 is the background Maxwellian distribution function, and T_{0j} is the background temperature. In addition, $\chi_j = \bar{\phi}_j + v_{Tj} v_{||} \bar{A}_{||_j}$, where the overbar denotes a gyroaverage, and v_{Tj} is the particle thermal velocity. The corresponding energy evolution equation is

$$\partial_t E_k = \mathcal{L}[g_k, g_k] + \sum_{k'_x, k'_y} \mathcal{N}[g_k, g_{k'}, g_{k-k'}] + c.c., \qquad (2)$$

where $\mathcal{L}$ includes the linear gyrokinetic operater, and the nonlinear energy transfer function $\mathcal{N}$ is defined as,

$$\mathcal{N}_{k,k'} = \sum_j \int dz dv_{||} d\mu \left(k'_x k_y - k_x k'_y\right) [q_j F_0/T_{0j} \qquad (3)$$
$$\chi^*_j(k)\chi_j(k')g_j(k-k') - g^*_j(k)\chi_j(k-k')g_j(k')] \quad .$$

The latter represents the energy transferred conservatively between the wavenumbers (k_x, k_y) and (k'_x, k'_y) as evidenced by the property, $\mathcal{N}_{k,k'} = -\mathcal{N}_{k',k}$. This, however, defines the nonlinear energy transfer function for all fluctuations at a given wavenumber; a refinement is necessary to examine the energetics of the tearing mode of interest: $\partial_t E^{(tear)}_{k_x,k_y} = \mathcal{L}[g^{(tear)}_{k_x,k_y}, g_{k_x,k_y}] + \sum_{k'_x,k'_y} \mathcal{N}[g^{(tear)}_k, g_{k'}, g_{k-k'}]$, where $g^{(tear)}$ represents the POD tearing mode described above, and the LHS represents the evolution of the tearing mode energy because of the orthogonality of the POD modes. It is observed that the nonlinear energy transfer for the tearing mode is dominated by energy injected *into* the mode from wavenumbers at the same k_y and $|k_x| > 0$, and energy transfered *out* of the mode into zonal wavenumbers ($k_y = 0$). Note that both of these energy transfer channels represent coupling with zonal wavenumbers. A closer examination shows that the energetics of the mode is dominated by the imbalance between this energy transfer as demonstrated in Fig. 3 where the free energy of the tearing mode is plotted along with the the total nonlinear drive and the component of the nonlinear drive defined by the subset of wavenumbers representing zonal coupling: $k'_y\rho_s = 0.2$ and $k'_y\rho_s = 0$. This subset captures the major trends in the energy balance. The linear term in the energy equation (not shown in Fig. 3) occasionally plays a role but is, in general, much smaller than the nonlinear term which dominates both the drive and saturation of the tearing mode. We thus have the unique situation where the saturation mechanism for the driving ITG instability in turn produces a significant additional transport channel.

One may now ask if this POD tearing mode finds an analog in the linear eigenmode spectrum. An examination of the linear spectrum reveals several classes of subdominant modes with tearing parity. There are several marginally stable tearing parity modes which are essentially electrostatic in nature. In order to find a mode which produces the transport described above, we employ a direct eigenvalue solver (incorporated into the GENE code) that resolves all eigenmodes in the spectrum, but is very numerically demanding. A reduced resolution test case [$(16, 32, 8)$ grid points in $(z, v_{||}, \mu)$] reveals one eigenmode which has a mode structure matching the POD mode described above and also produces a significant amount of electromagnetic transport. A series of numerical tests indicate that this mode is a legitimate microtearing mode similar to those described in Refs. [13, 14]: the mode is sensitive to changes in the electron temperature gradient but not the ion temperature gradient, it is fundamentally changed in the electrostatic limit but not when the electrostatic potential is artificially deleted. The distribution function from a corresponding nonlinear run was projected onto a large set of orthogonalized eigenmodes and the contribution of each to the electromagnetic heat transport was calculated. The results are shown in Fig. 4 where the eigenvalues are plotted in the complex plane representing the mode growth rates and frequencies, and the color weighting indicates the absolute value of the electromagnetic transport produced by each mode. The ITG mode is associated with a large negative value and the subdominant tearing mode [with $\gamma(R/c_s) = -0.43$ and $\omega(R/c_s) = -0.98$] produces a sig-

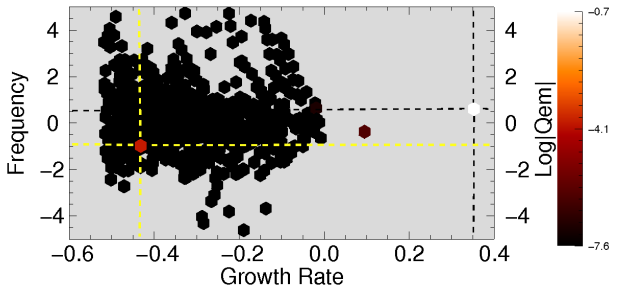

FIG. 4: Plot of a subset of linear eigenvalues ($k_y\rho_s = 0.2, k_x\rho_s = 0$, and $\beta = 0.003$) color weighted by the absolute value of their contribution to the electromagnetic electron heat flux. The ITG mode and the subdominant microtearing mode produce the only non-negligible contributions to the magnetic transport.

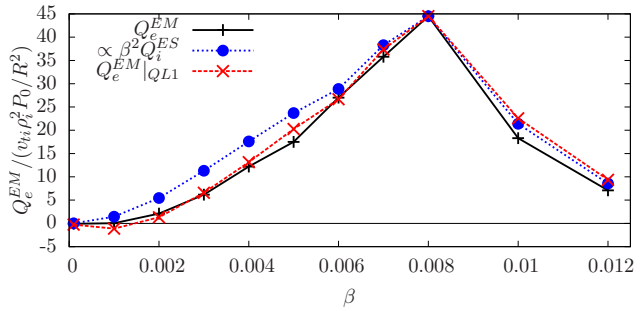

FIG. 5: Q_e^{EM} plotted over the β scan (plus signs) along with a model estimating the flux as a fixed fraction of $\beta^2 Q_i^{ES}$ (circles), and a model with an additional correction (crosses) defined by the quasilinear magnetic flux associated with the most unstable mode (ITG at lower β and TEM at higher β).

nificant positive value. All other modes are negligible with regard to electromagnetic transport. For this problem, linear convergence tests are, ironically, more demanding than nonlinear convergence tests. Careful nonlinear convergence tests were performed and reported in Ref. [4]. These tests have been augmented by a high k_x resolution GENE simulation ($k_{x_{max}}\rho_s = 11.9$) which shows no significant change in the transport quantities.

The transport scenario described above defines a significant component of the transport which is not directly attributable to the driving instabilities. It is, rather, associated with subdominant, nonlinearly excited fluctuations whose saturation level is set by nonlinear energy balances. One might expect such a situation to be difficult to model with quasilinear theory, as is noted in Ref. [4]. Here we describe a simple model that captures the β dependence of the of Q_e^{EM} using as inputs the ion electrostatic heat flux and one free parameter that can be determined at a single point in the scan.

The nonlinear nature of the tearing mode excitation motivates the hypothesis that the level of electron electromagnetic heat flux (due to the nonlinearly driven tearing modes) can be modelled as a fixed fraction of the ion electrostatic heat transport (due to the dominant instabilities) multiplied by the appropriate factor of β^2: $Q_e^{EM}(\beta) = C_0\beta^2 Q_i^{ES}$. In Fig. 5, this estimate is plotted across the β scan along with the total value of Q_e^{EM} (C_0 is calculated at $\beta = 0.008$). This model model can be improved by also accounting for the contribution of the ITG modes themselves to Q_e^{EM}. This is done with the quasilinear estimate: $Q_e^{EM(ball)} = Q_i^{ES}\left\{\frac{Q_e^{EM}}{Q_i^{ES}}\right\}_{MU}$, where $\left\{\frac{Q_e^{EM}}{Q_i^{ES}}\right\}_{MU}$ is the ratio of fluxes for the most unstable linear eigenmode (ITG at lower β and trapped electron mode (TEM) at higher β) at the peak of the spectrum ($k_y\rho_s = 0.15$). This estimate, $Q_e^{EM} = Q_i^{ES}\left(C_0\beta^2 + \left\{\frac{Q_e^{EM}}{Q_i^{ES}}\right\}_{MU}\right)$, is also plotted in Fig. 5. The merit of this quasilinear refinement is reflected in the improved agreement at lower β where the inward ballooning transport is a non-negligible fraction of the whole.

In summary, we have shown that magnetic stochasticity and transport in ITG driven turbulence is cause by subdominant microtearing modes which are nonlineary excited by coupling to zonal wavenumbers. The resulting transport can be modelled as a fixed fraction of the transport associated with the driving instabilities.

Simulation results were obtained using computing resources on the HPC-FF system at Forschungszentrum Jülich, Germany; and NCCS at ORNL, USA under DOE contract No. DE-AC05-00OR22725. This work was also supported by LLNL through DOE contract No. DE-AC52-07NA27344.

[1] F. Jenko *et al.*, Phys. Plasmas **7**, 1904 (2000).
[2] S. E. Parker *et al.*, Phys. Plasmas **11**, 2594 (2004).
[3] J. Candy, Phys. Plasmas **12**, 072307 (2005).
[4] M. J. Pueschel, M. Kammerer, F. Jenko, Phys. Plasmas **15**, 102310 (2008).
[5] M. J. Pueschel and F. Jenko, Phys. Plasmas **17**, 062307 (2010).
[6] A. M. Dimits *et al.*, Phys. Plasmas **7**, 969 (2000).
[7] M.J. Pueschel, Ph.D. thesis, Universität Münster, (2009).
[8] W. M. Nevins *et al.*, Phys. Rev. Lett. **106**, 065003 (2011).
[9] E. Wang *et al.*, Phys. Plasmas **18**, 056111 (2011).
[10] P. W. Terry *et al.*, Phys. Plasmas **13**, 022307 (2006).
[11] D. R. Hatch *et al.*, Phys. Rev. Lett. **106**, 115003 (2011).
[12] D. R. Hatch *et al.*, Phys. Plasmas **18**, 055706 (2011).
[13] H. Doerk *et al.*, Phys. Rev. Lett. **106**, 155003 (2011).
[14] W. Guttenfelder *et al.*, Phys. Rev. Lett. **106**, 155004 (2011).
[15] G. Berkooz, P. Holmes, and J. L. Lumley, Annu. Rev. Fluid Mech. 25, 539-575 (1993).
[16] S. Futatani *et al.*, Phys. Plasmas **16**, 042506 (2009).
[17] M. A. Beer *et al.*, Phys. Plasmas **2**, 2687 (1995).
[18] C. Holland *et al.*, Nucl. Fusion **43**, 761 (2003).